Research Square

Preprints are preliminary reports that have not undergone peer review.
They should not be considered conclusive, used to inform clinical practice,
or referenced by the media as validated information.

Modified Anshen Dingzhi Prescription Ameliorates Tourette Syndrome and Comorbid Anxiety by Modulating Synaptic Plasticity and the cAMP/PKA/CREB Signaling Pathway

Si Zhang
Suzhou TCM Hospital, Nanjing University of Chinese Medicine
Lixiang Zhang
Children's Hospital of Soochow University
Yan Li
Suzhou TCM Hospital, Nanjing University of Chinese Medicine
Mei Li
Children's Hospital of Soochow University
Jie Chen
Suzhou TCM Hospital, Nanjing University of Chinese Medicine
Liang Li
Children's Hospital of Soochow University
Fei Fan
China Academy of Chinese Medical Sciences
Xiaohua Shen
Suzhou TCM Hospital, Nanjing University of Chinese Medicine
Guoqiang Liang
Suzhou TCM Hospital, Nanjing University of Chinese Medicine
Lingling Yang
yanglingling1116@163.com

Suzhou TCM Hospital, Nanjing University of Chinese Medicine

Research Article

Keywords: Modified Anshen Dingzhi Prescription, Tourette Syndrome, Anxiety, Synaptic plasticity, cAMP/PKA/CREB signaling pathway, Integrated pharmacology

Posted Date: August 11th, 2026

DOI: https://doi.org/10.21203/rs.3.rs-10174946/v1

License: This work is licensed under a Creative Commons Attribution 4.0 International License.
Read Full License

Additional Declarations: No competing interests reported.

Modified Anshen Dingzhi Prescription Ameliorates Tourette Syndrome and Comorbid Anxiety by Modulating Synaptic Plasticity and the cAMP/PKA/CREB Signaling Pathway

Si Zhang [1], Lixiang Zhang [2], Yan Li [1], Mei Li [2], Jie Chen [1], Liang Li [3], Fei Fan [4], Xiaohua Shen [1], Guoqiang Liang [1,5], and Lingling Yang [1,*]

[1]Department of Pediatrics, Suzhou TCM Hospital Affiliated to Nanjing University of Chinese Medicine, Suzhou, Jiangsu, China.
[2]Department of Neonatology, Children's Hospital of Soochow University, Suzhou, Jiangsu, China.
[3]Department of Integrated Traditional Chinese and Western Medicine, Children's Hospital of Soochow University, Suzhou, Jiangsu, China.
[4]Department of Pediatrics, Guang'anmen Hospital, China Academy of Chinese Medical Sciences, Beijing, China.
[5]Suzhou Academy of Wumen Chinese Medicine, Suzhou, Jiangsu, China.

*Correspondence: Lingling Yang, Department of Pediatrics, Suzhou TCM Hospital Affiliated to Nanjing University of Chinese Medicine, No. 18 Yangsu Road, Gusu District, Suzhou 215009, Jiangsu Province, China, Email: yanglingling1116@163.com

Abstract

Background Tourette Syndrome (TS) are complex neurodevelopmental conditions frequently comorbid with anxiety. Modified Anshen Dingzhi Prescription (MADP), an empirical Chinese herbal formula, has demonstrated dual therapeutic benefits in suppressing tics and regulating emotions; however, its multi-component mechanisms remain to be fully elucidated.
Objective This study investigated the therapeutic efficacy of MADP on TS comorbid with anxiety and explored its molecular mechanisms involving prefrontal cortex (PFC) synaptic plasticity and the cAMP/PKA/CREB signaling pathway.
Methods A rat model of TS comorbid with anxiety was induced by 3,3'-iminodipropionitrile (IDPN) and chronic restraint stress (CRS). Therapeutic effects were assessed using stereotypic behavior scores and the open field test (OFT). PFC neuronal morphology and dendritic spine density were observed through Nissl and Golgi staining. Chemical profiling of MADP was performed via UPLC-MS/MS. Integrated network pharmacology and transcriptomics were employed to predict hub targets and pathways, followed by validation using Western blot and immunofluorescence.
Results MADP treatment significantly attenuated stereotypic behavior scores and improved abnormal activity patterns. Pathological observations revealed that MADP effectively restored neuronal integrity in the PFC, significantly increasing dendritic spine density, total neurite length, and dendritic arbor complexity. UPLC-MS/MS identified 135 bioactive constituents. Multi-omics integration indicated that the cAMP signaling pathway is a critical intervention route. Molecular validation demonstrated that MADP significantly upregulated protein levels of PKA and CREB, enhanced CREB

phosphorylation (p-CREB), and increased the expression of the synaptic markers PSD95 and Synapsin I+II (P<0.05).

Conclusion MADP effectively ameliorates behavioral symptoms in TS comorbid with anxiety by activating the cAMP/PKA/CREB signaling pathway and restore PFC synaptic plasticity. These findings provide scientific mechanistic evidence supporting the clinical application of MADP.

Keywords Modified Anshen Dingzhi Prescription; Tourette Syndrome; Anxiety; Synaptic plasticity; cAMP/PKA/CREB signaling pathway; Integrated pharmacology

1. Introduction

Tourette Syndrome (TS) is a complex, childhood-onset neuropsychiatric disorder primarily characterized by repetitive motor and vocal tics.[1] Emerging evidence suggests that TS should not be regarded merely as an isolated challenge of tic control; rather, its clinical essence involves an intricate network of psychopathological comorbidities, which affect over 50% of pediatric patients.[2] Within this comorbid spectrum, attention-deficit/hyperactivity disorder (ADHD) and obsessive-compulsive disorder (OCD) have been extensively investigated.[3,4] However, anxiety, another high-prevalence comorbidity with incidence rates ranging from 31.4% to 72.7%, is increasingly being recognized for its significant contribution to the overall disease burden.[5] Notably, while tics often undergo spontaneous attenuation as patients transition into adulthood, comorbid anxiety frequently persists. This persistence not only severely compromises the quality of life and escalates subjective distress but also heightens the risk of suicidal ideation and behavior.[6,7]

Currently, α2-adrenergic receptor agonists and antipsychotic medications remain the primary pharmacological options for tic suppression, sometimes supplemented by agents such as sertraline to manage comorbid anxiety.[8] Nevertheless, these conventional interventions are frequently constrained by the dual challenges of limited clinical efficacy and suboptimal tolerability. Moreover, most existing medications struggle to simultaneously meet the therapeutic demands of controlling tics while effectively alleviating comorbid anxiety.[5] Consequently, there is a paramount clinical urgency to explore safe and effective alternative strategies that can concurrently address both tics and comorbidities.

According to the theory of Traditional Chinese Medicine (TCM), the tics of TS are primarily categorized as internal stirring of liver wind (Gan Feng Nei Dong), whereas comorbid emotional disturbances, such as anxiety and panic, are attributed to an unsettled heart-spirit (Xin Shen Bu Ning). Guided by the fundamental TCM principle of syndrome differentiation and treatment (Bian Zheng Lun Zhi), a therapeutic strategy that concurrently prioritizes extinguishing liver wind and tranquilizing the heart to calm the spirit is essential for this complex spectrum. Modified Anshen Dingzhi Prescription (MADP) was developed by integrating clinical experience with the classic prescriptions Xiaoyaosan and Anshen Dingzhi Pill. Comprising nine botanical herbs (Table 1), MADP is designed to extinguish liver wind, clear heart-fire, and stabilize the spirit. Previous clinical observations have demonstrated that MADP exhibits significant efficacy in ameliorating tics and improving overall behavioral outcomes.[9,10]

While MADP's multi-component mechanisms are not fully elucidated, its core herb pairs are pharmacologically supported. Formulations centered on the combination of *Bupleurum chinense* and *Paeonia lactiflora* have been demonstrated to alleviate tic behaviors by mitigating hippocampal oxidative stress.[11] Bioactive α-asarone and polygalasaponins from *Acori Tatarinowii Rhizoma* and

Polygalae Radix activate BDNF-TrkB and mTOR-dependent synaptic plasticity to ameliorate stress-induced deficits.[12,13] Additionally, the *Acori Tatarinowii* and *Curcuma wenyujin* combination enhances cognition and alleviates depression via AMPK activation and neuroinflammation suppression.[14,15] These findings provide a scientific rationale for investigating the synaptic modulatory and neuroprotective potential of MADP.

This study aims to investigate the therapeutic efficacy and molecular mechanisms of MADP in TS with comorbid anxiety. A rat model was established via iminodipropionitrile (IDPN) injection and chronic restraint stress (CRS). Treatment effects were characterized using behavioral analysis, Golgi staining, and Nissl staining. Chemical profiling of MADP was performed via UPLC-MS/MS. An integrated approach combining transcriptomics, network pharmacology, Western blotting, and immunofluorescence was then used to investigate its therapeutic mechanisms. These findings provide a robust experimental basis for the clinical application of MADP.

2. Materials and methods

2.1. Preparation of MADP

The herbal components of MADP are summarized in Table 1. All herbal medicines were purchased from the Suzhou TCM Hospital Affiliated to Nanjing University of Chinese Medicine (Suzhou, China) and were authenticated according to the standards of the Chinese Pharmacopoeia (ChP, 2020 edition). The herbal ingredients were weighed and soaked in 10 volumes of distilled water (w/v) for 30 min. The mixture was initially boiled under high heat and then simmered for 1 h. After filtration, the residue was decocted a second time with 8 volumes of distilled water for 45 min. The two filtrates were combined and concentrated to a final density of 1 g/mL using a rotary evaporator. The resulting MADP extract was stored at 4°C.

Table 1 The List of Herbal Compositions in MADP

Herbal Name	Herbal Name in Chinese	Dosage
Acorus tatarinowii Schott	Shichangpu	10g
Polygala tenuifolia Willd.	Yuanzhi	10g
Bupleurum chinense DC.	Chaihu	10g
Scutellaria baicalensis Georgi	Huangqin	10g
Paeonia lactiflora Pall.	Baishao	10g
Curcuma wenyujin Y.H.Chen et C.Ling	Yujin	10g
Chrysanthemum morifolium Ramat.	Juhua	6g
Cryptotympanapustulata Fabricius	Chantui	6g
Cassia obtusifolia L.	Juemingzi	10g

2.2. Chemical profiling of MADP

Qualitative analysis of the MADP aqueous extract was performed using a UPLC-MS/MS system. Chromatographic separation was achieved on a U3000 ultra-performance liquid chromatography system (Thermo Fisher Scientific, USA) equipped with a Waters ACQUITY UPLC HSS T3 column (2.1 × 100 mm, 1.8 μm). The analytical conditions were set as follows: column temperature, 35°C;

flow rate, 0.3 mL/min; and injection volume, 10 μL. The mobile phase comprised 0.1% (v/v) aqueous formic acid (A) and 0.1% (v/v) formic acid in acetonitrile (B). The 70-min gradient elution program was optimized as follows: 0–45 min, 0%–100% B; 45–60 min, 100% B; 60–60.5 min, 100%–0% B; and 60.5–70 min, 0% B.

Mass spectrometry analysis was conducted using a Q Exactive Plus Orbitrap high-resolution mass spectrometer (Thermo Fisher Scientific) operated in both positive and negative ion modes using a Full MS-ddMS2 scan strategy. Data were acquired across a mass range of m/z 100–1200. The key acquisition parameters were optimized as follows: MS1 and MS2 resolutions, 70,000 and 17,500, respectively; spray voltage, 3.2 kV; capillary temperature, 320°C; auxiliary gas temperature, 350°C; and stepped normalized collision energy (NCE), 30, 40, and 50. The raw data were analyzed using Compound Discoverer 3.2 software (Thermo Fisher Scientific) for feature peak extraction with a mass tolerance of < 5 ppm. Chemical constituents were identified by matching fragmentation patterns against the mzCloud online database and a local mzVault database. Only identification results with a matching score of ≥ 70 were retained for further analysis.[16]

2.3. Animals and model establishment

Specific pathogen-free (SPF) male Sprague-Dawley (SD) rats (3 weeks old, weighing 40–60 g) were obtained from Hangzhou Qizhen Experimental Animal Technology Co., Ltd. [production license number: SCXK (Zhe) 2022-0005]. All rats were housed in a standard controlled barrier environment at a temperature of 22 ± 2°C and a relative humidity of 40%–60%, with a 12-h light/dark cycle and ad libitum access to food and water. After one week of acclimatization, the experimental procedures were initiated.

To induce the TS with comorbid anxiety model, rats were administered daily intraperitoneal (i.p.) injections of 3,3'-iminodipropionitrile (IDPN) (Sigma-Aldrich, HPLC ≥ 90%, 317306) at a dose of 250 mg/kg/day from days 0 to 7 to elicit typical motor tic symptoms.[17] Concurrently, from days 0 to 28, the rats were subjected to chronic restraint stress (CRS) by being placed in specialized restraint cylinders for 3 h daily (9:00 AM – 12:00 PM) to induce chronic psychological stress via spatial restriction.[18,19] Conversely, the control group received saline injections and remained unrestrained in their home cages.

2.4. Grouping and drug administration

From days 8 to 28, rats were randomly assigned into five experimental groups (n = 15 per group): (1) Control group; (2) IDPN + CRS group (Model); (3) IDPN + CRS + MADP low-dose group (MADP-L); (4) IDPN + CRS + MADP high-dose group (MADP-H); and (5) IDPN + CRS + Tiapride group (Tiapride). The Control and Model groups were administered saline (10 mL/kg/day) via oral gavage for 3 weeks. The MADP-L and MADP-H groups received MADP extract at doses of 8.54 g/kg/day and 17.08 g/kg/day, respectively. The Tiapride group was administered Tiapride (31.25 mg/kg/day; Jiangsu Nhwa Pharmaceutical Co., Ltd., China; H32025477). Dosage calculation was based on the body surface area ratio between humans and rats. The MADP-L dose corresponded to the clinical equivalent dose, while the MADP-H dose was twice the clinical equivalent.

2.5. Behavioral assessments

Stereotypic behaviors were evaluated on days 8 and 28 based on the Diamond scoring method. The

scoring criteria were defined as follows: 0, no stereotypic behavior; 1, circling behavior; 2, excessive vertical head and neck movements; 3, vertical head/neck movements combined with circling; 4, head shaking combined with excessive vertical head/neck movements. Rats were observed for 1 min every 5 min over a 30-min period (totaling six observation intervals), and the scores were recorded by an observer blinded to the experimental groups.[20]

Anxiety-like behaviors were assessed using the open field test (OFT) on day 28. Prior to testing, rats were moved to the behavioral testing room in their home cages for 30 min. During the test, each rat was placed in the center area of the open field box and allowed to explore freely for 5 min. An automated behavior analysis system (Shanghai Xinruan Information Technology Co., Ltd., China) was used to track and record the following parameters: total distance, average speed, center distance, central time and number of center entries. After each trial, the arena was thoroughly cleaned with 75% ethanol to eliminate residual odors and excrement.

2.6. Nissl staining

Following behavioral assessments, rats were anesthetized with 5% isoflurane and rapidly decapitated for whole-brain tissue collection. The brain tissues were paraffin-embedded and sectioned using a microtome (RM2016, Leica, Germany). Sections were deparaffinized in xylene and rehydrated through a graded ethanol series. Subsequently, the sections were stained with Nissl staining solution (G1036, Servicebio, China) for 2 min, briefly differentiated in 1% glacial acetic acid for 1 s, and rinsed with tap water to terminate the reaction. After being thoroughly oven-dried, the sections were cleared in xylene for 15 min and mounted with neutral resin. Finally, images of deep-blue Nissl bodies were observed and captured using a light microscope (Eclipse E100, Nikon, Japan) equipped with a digital imaging system (DS-U3, Nikon, Japan).

2.7. Golgi staining

Fresh whole-brain tissues were immersed in Golgi fixative (G1069, Servicebio) and kept in the dark for 1–5 days. After being rinsed with PBS, the tissues were incubated in Golgi staining solution for 14 days, with the solution replaced after the first 48 h and subsequently every 3 days. The brains were then cut into 60-μm-thick sections using a vibrating microtome (VT1000S, Leica, Germany). The sections were mounted on slides, air-dried overnight at 4°C, and then developed in concentrated ammonia for 10 min. Following a distilled water wash, the slices were mounted with glycerol-gelatin medium. Finally, multilayer images were captured using a digital scanner (LG-S80, Servicebio).

2.8. Network pharmacology analysis

Based on the UPLC-MS/MS identification results, the canonical SMILES strings of the chemical constituents in MADP were retrieved from the PubChem database (https://www.ncbi.nlm.nih.gov/). Potential targets were predicted using the Swiss Target Prediction tool (http://swisstargetprediction.ch/), with the species restricted to "Homo sapiens" and a probability threshold > 0.

Disease-related targets for TS and anxiety were collected from the GeneCards, OMIM, TTD, PharmGkb, and DisGeNET databases. The intersection of compound-related and disease-related targets was identified using the Jvenn online tool, and a compound-target network was constructed using Cytoscape software (v3.10.4). Subsequently, these overlapping targets were imported into the

STRING database (https://cn.string-db.org/) to construct a protein-protein interaction (PPI) network, with a minimum required interaction confidence score of ≥ 0.900. The CytoNCA plugin was utilized to perform topological analysis. Core targets were screened based on the median values of six parameters: betweenness centrality (BC), closeness centrality (CC), degree centrality (DC), eigenvector centrality (EC), network centrality (NC), and local average connectivity (LAC).
Gene Ontology (GO) and Kyoto Encyclopedia of Genes and Genomes (KEGG) pathway enrichment analyses were conducted using the clusterProfiler package in R (v4.1.3). An adjusted $P < 0.05$ was considered statistically significant. The enrichment results were visualized using the enrichplot and ggplot2 R packages.

2.9. Transcriptomic analysis

Total RNA was extracted from rat prefrontal cortex (PFC) tissues using TRIzol reagent (Invitrogen, USA), and its integrity and quantity were assessed using an Agilent 2100 Bioanalyzer. mRNA was enriched from total RNA using oligo(dT) magnetic beads, followed by double-stranded cDNA synthesis, end repair, A-tailing, and adapter ligation. The resulting cDNA fragments (approximately 370–420 bp) were purified using AMPure XP beads and amplified via PCR. Library quality was validated using the Agilent 2100 system and precisely quantified by qRT-PCR (effective concentration > 1.5 nM). Qualified libraries were pooled and sequenced on the Illumina NovaSeq X Plus platform. Raw sequencing data underwent quality control and alignment to obtain clean, valid data. Differential expression analysis was performed using the DESeq2 R package (v1.20.0), and genes with $P < 0.05$ were defined as differentially expressed genes (DEGs). GO and KEGG enrichment analyses were conducted using the clusterProfiler R package (v3.8.1). An adjusted $P < 0.05$ was considered statistically significant.

2.10. Western blot

Total proteins were extracted from PFC tissues using RIPA lysis buffer supplemented with protease and phosphatase inhibitors (G2002, Servicebio). Protein concentrations were determined using a BCA protein assay kit (G2026, Servicebio). Equivalent amounts of protein were separated by SDS-PAGE and subsequently transferred onto PVDF membranes (G6047, Servicebio). The membranes were then rapidly blocked at room temperature for 10 min. Next, the membranes were incubated overnight at 4°C with the following primary antibodies: anti-β-tubulin (1:5000, GB15140, Servicebio), anti-p-PKACA (1:1000, R015300, Yamei, China), anti-PKACA (1:1000, GB11598, Servicebio), anti-p-CREB (1:1000, GB114322, Servicebio), and anti-CREB (1:1000, GB111052, Servicebio). After three washes with TBST, the membranes were incubated with HRP-conjugated goat anti-rabbit secondary antibody (1:3000, GB23303, Servicebio) for 30 min at room temperature. Finally, the protein bands were visualized using an ECL chemiluminescence kit (Servicebio) and captured with a chemiluminescence imaging system (SCG-W3000 PLUS, Servicebio). The gray values of the bands were quantified using AIWBwell™ software (Servicebio). Target protein levels were normalized to the internal control, β-tubulin.

2.11. Immunofluorescence

Deparaffinized rat brain sections were subjected to antigen retrieval in Tris-EDTA buffer (pH 8.0) for 30 min. Following the quenching of endogenous peroxidase activity with 3% H2O2 and blocking with

3% BSA, dual labeling of homologous rabbit antibodies was performed using the Tyramide Signal Amplification (TSA) technique. Sections were first incubated with anti-Synapsin I+II (1:1000, HA723196, HUABIO) overnight at 4 °C. After thorough washing, the sections were incubated with an HRP-conjugated goat anti-rabbit secondary antibody (G1302, Servicebio) for 50 min at room temperature, followed by signal amplification using iF555-Tyramide (Servicebio) for 10 min. Subsequently, the sections were incubated with the second primary antibody, anti-PSD95 (1:500, GB11277, Servicebio), overnight at 4 °C. Following a second 50-min incubation with the HRP-conjugated secondary antibody, signal amplification was conducted with iF488-Tyramide (Servicebio) for 10 min. Finally, nuclei were counterstained with DAPI, and autofluorescence was quenched using a specialized reagent (G1221, Servicebio). Images were captured utilizing a digital slide scanner (Pannoramic MIDI, 3DHISTECH, Hungary).

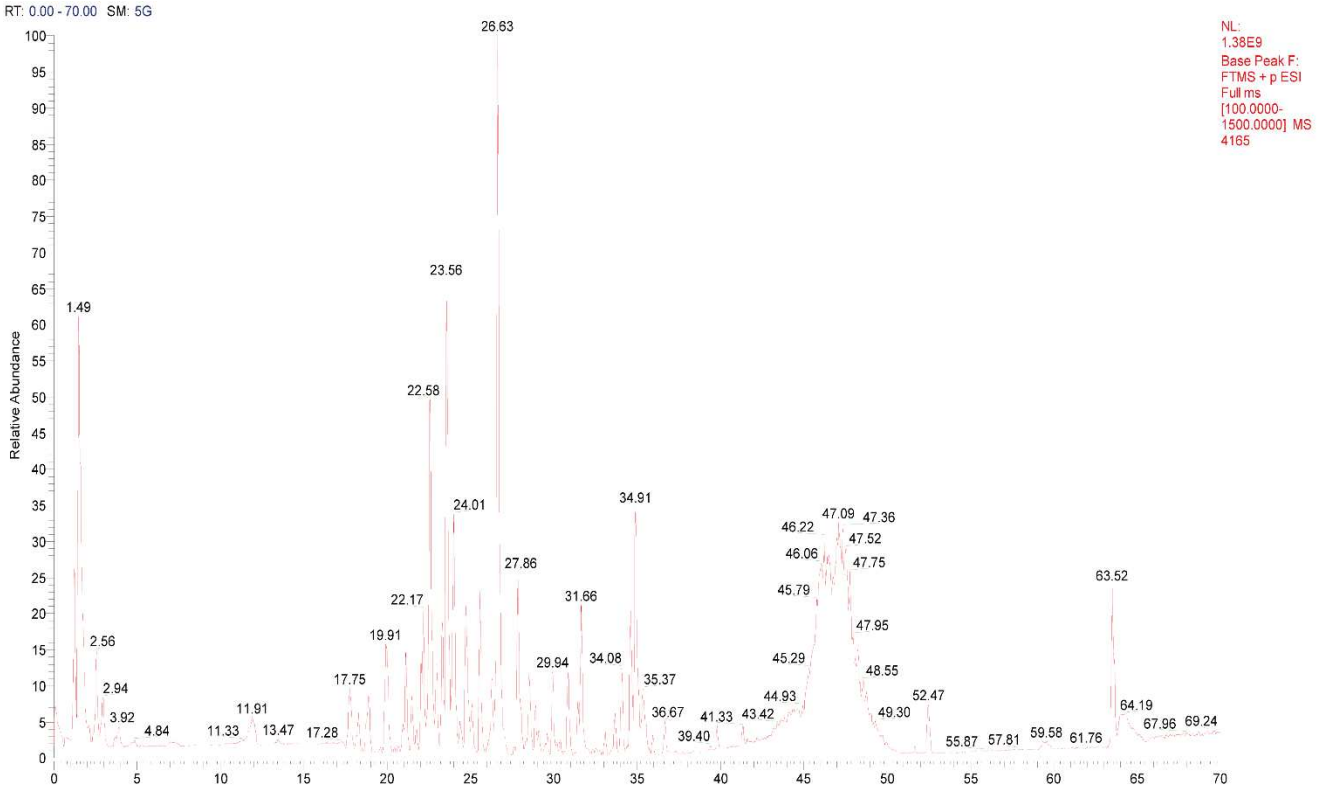
2.12. Statistical analysis

All quantitative results are presented as means ± standard error of the mean (SEM). Statistical analyses were conducted using GraphPad Prism software (version 9.0; GraphPad Software Inc., USA). For comparisons involving three or more groups, one-way or two-way analysis of variance (ANOVA) was employed, followed by Tukey's post hoc test to evaluate the significance of findings. A $P < 0.05$ was considered to indicate statistical significance.

3. Results

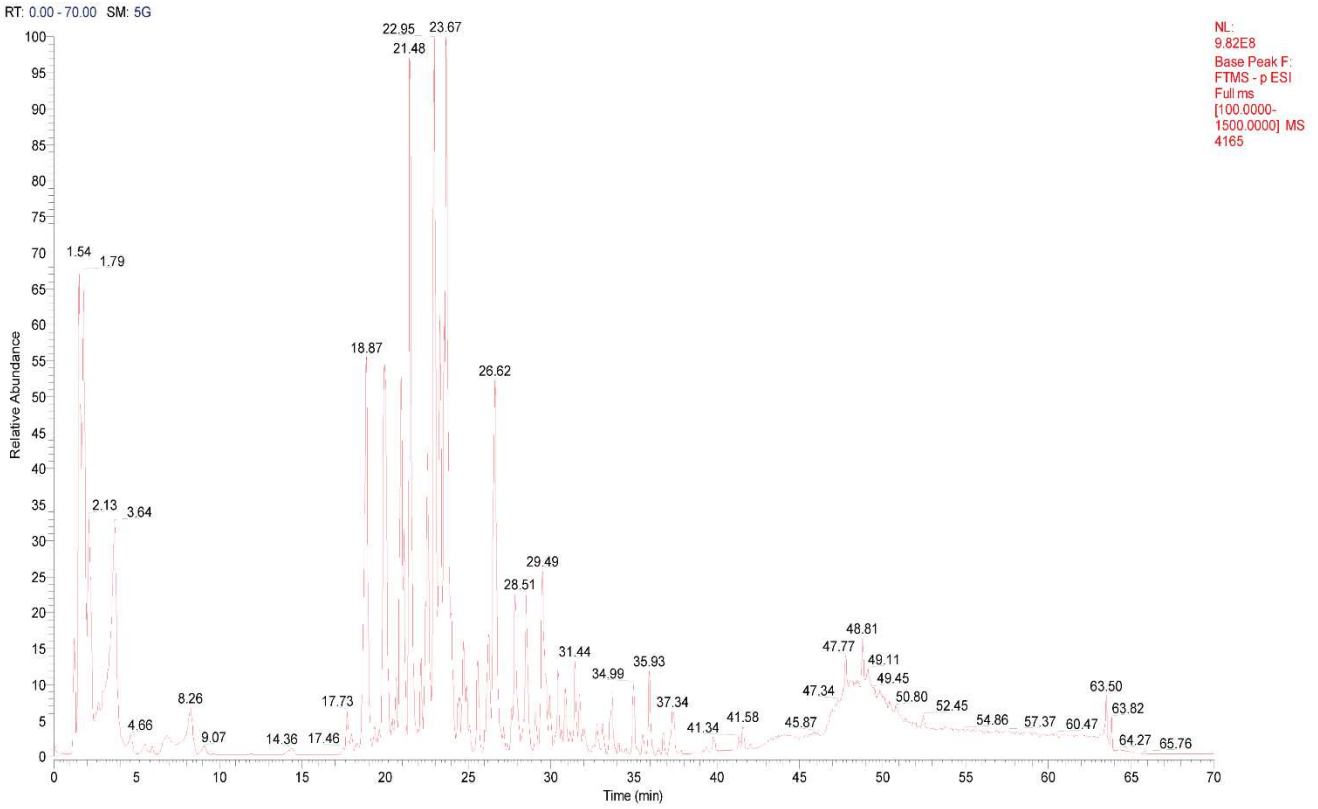
3.1. Chemical constituents of MADP

Chemical profiling of MADP was performed using a UPLC-MS/MS system, with the acquired data matched against the mzVault database. A matching score threshold of 70 was applied for compound screening. A total of 135 compounds were identified, including saikosaponin A, paeoniflorin, tenuifolin, and α-asarone. The total ion chromatograms (TIC) in both positive and negative ion modes are presented in Figures 1 and 2, respectively. A comprehensive list of the identified chemical components is provided in Supplementary Table S1.



252

253 **Fig. 1** TIC of MADP sample in positive ion mode



254

255 **Fig. 2** TIC of MADP sample in negative ion mode

256 **3.2. Behavioral assessments**

Compared to the control group, the model group exhibited significantly elevated stereotypic behavior scores on both days 8 and 28 ($P < 0.05$; Fig. 3). However, treatment with either MADP (low and high doses) or tiapride significantly attenuated these scores ($P < 0.05$). In the OFT, the model rats showed significant increases in total distance, average speed, and number of center entries ($P < 0.05$), likely driven by excessive stereotypic movements. While treatment with MADP or tiapride mitigated these parameters, they remained significantly higher than those of the control group ($P < 0.05$). Notably, unlike the typical anxiogenic effects induced by CRS alone, excessive stereotypic activity appeared to mask such behaviors, resulting in an increased frequency of center entries in model rats. These results are presented in Figure 4.

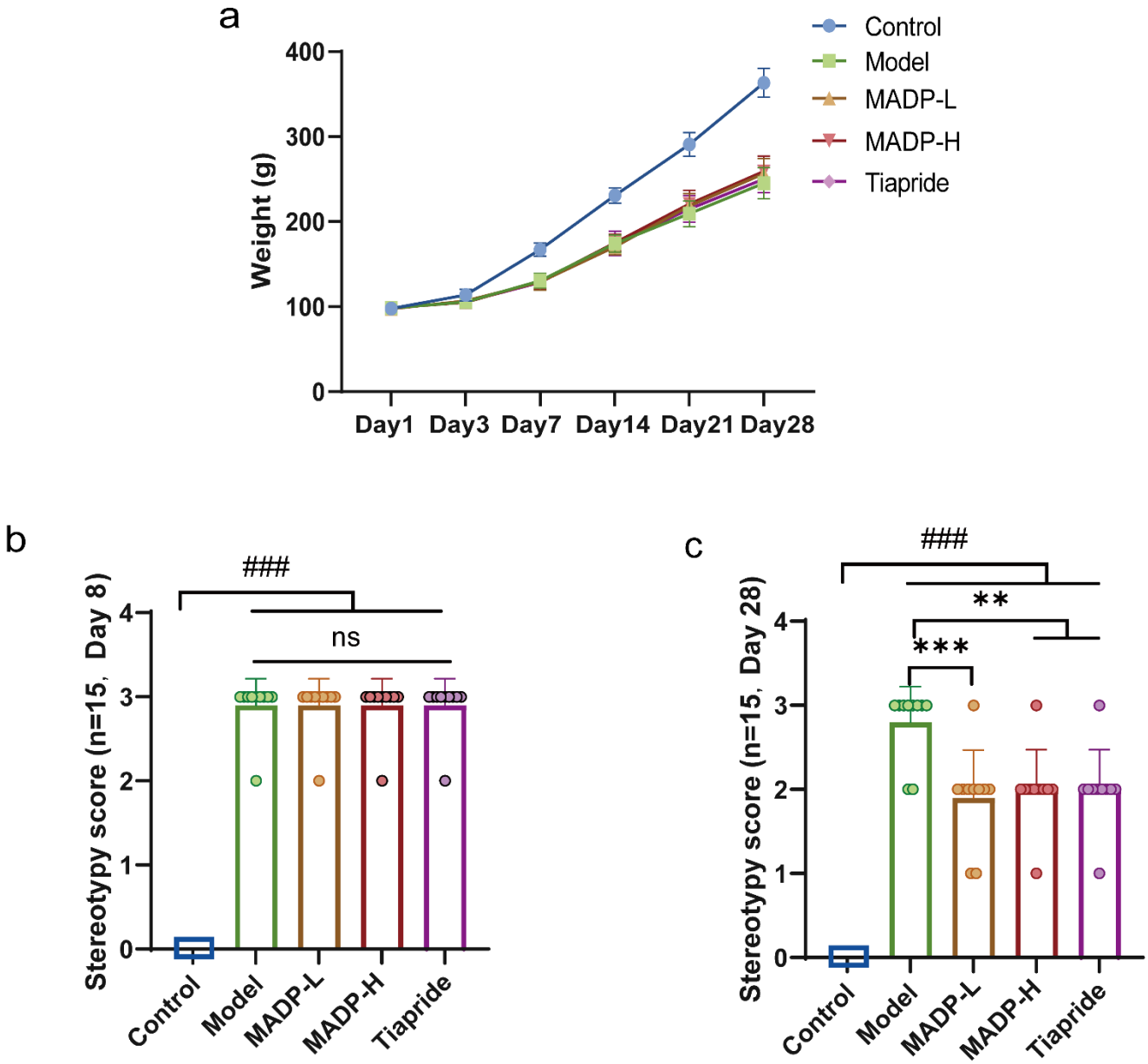
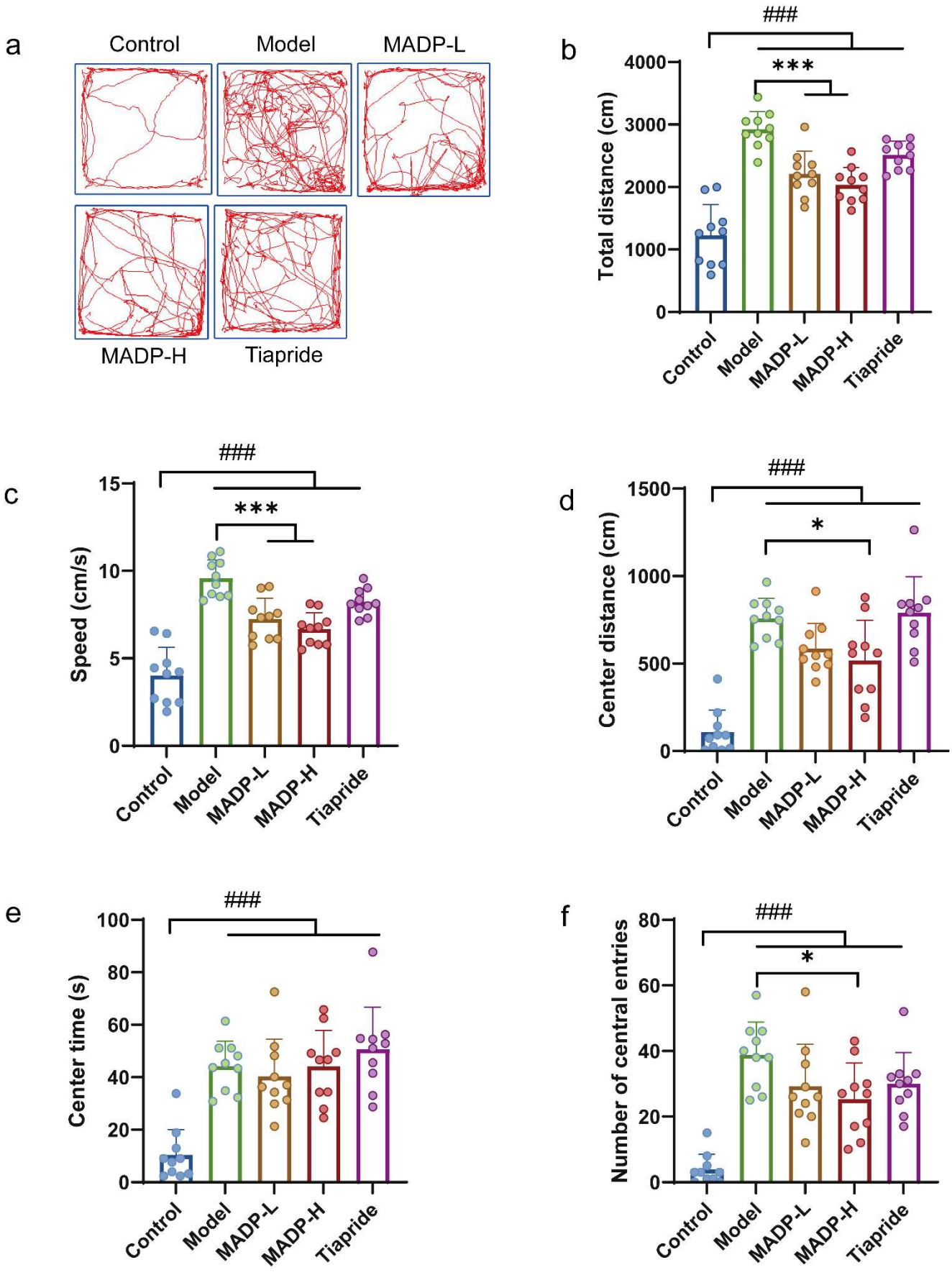


Fig. 3 Changes in body weight and stereotypic behavior scores across experimental groups (a)Body weight changes of rats from days 1 to 28. (b) Stereotypic behavior scores following one week of IDPN modeling. (c) Stereotypic behavior scores after three weeks of intervention. Data are presented as means ± SEM (n = 15 per group). The notation ns signifies no significant difference, while ###$p < 0.001$ indicates a comparison with the Control group. Conversely, **$p < 0.01$ and ***p

272 < 0.001 refer to comparisons with the Model group. All data were assessed using one-way ANOVA
273 followed by Tukey's multiple-comparisons test.


a
Control
Model
MADP-L
MADP-H
Tiapride
b
###
***
Total distance (cm)
4000
3000
2000
1000
0
Control
Model
MADP-L
MADP-H
Tiapride
c
###
***
Speed (cm/s)
15
10
5
0
Control
Model
MADP-L
MADP-H
Tiapride
d
###
*
Center distance (cm)
1500
1000
500
0
Control
Model
MADP-L
MADP-H
Tiapride
e
###
Center time (s)
100
80
60
40
20
0
Control
Model
MADP-L
MADP-H
Tiapride
f
###
*
Number of central entries
80
60
40
20
0
Control
Model
MADP-L
MADP-H
Tiapride

274

Fig. 4 Comparison of OFT results across experimental groups
(a) Representative movement trajectories in the OFT. (b–f) Quantitative analysis of total distance, average speed, center distance, central time, and number of center entries. Data are presented as means ± SEM. The notation ###$p < 0.001$ indicates a comparison with the Control group. Conversely, *$p < 0.05$ and ***$p < 0.001$ refer to comparisons with the Model group. All data were assessed using one-way ANOVA followed by Tukey's multiple-comparisons test.

3.3. Nissl staining

Nissl staining was employed to evaluate the alterations of neurons in the PFC. In the control group, neurons exhibited an orderly arrangement with abundant and clearly stained Nissl bodies within the cytoplasm. Conversely, the model group showed disorganized alignment, pale cytoplasmic staining, and signs of cellular swelling or pyknosis. Treatment with both MADP (low and high doses) and tiapride attenuated these pathological injuries and restored neuronal structural integrity. Although neuron counts per unit area in the treatment groups showed an upward trend compared to the model group, the differences did not reach statistical significance ($P > 0.05$). Representative details are presented in Figure 5.

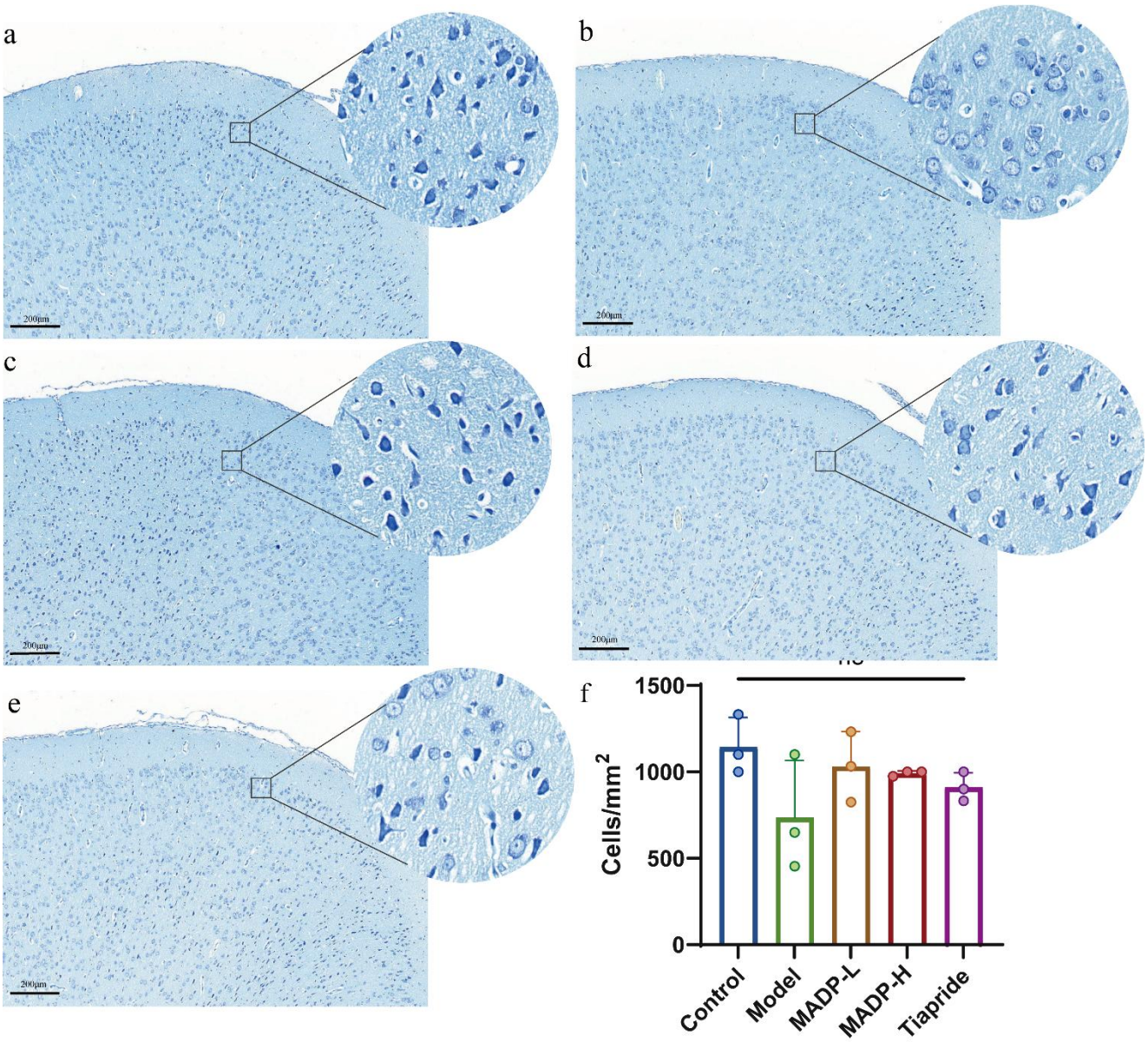
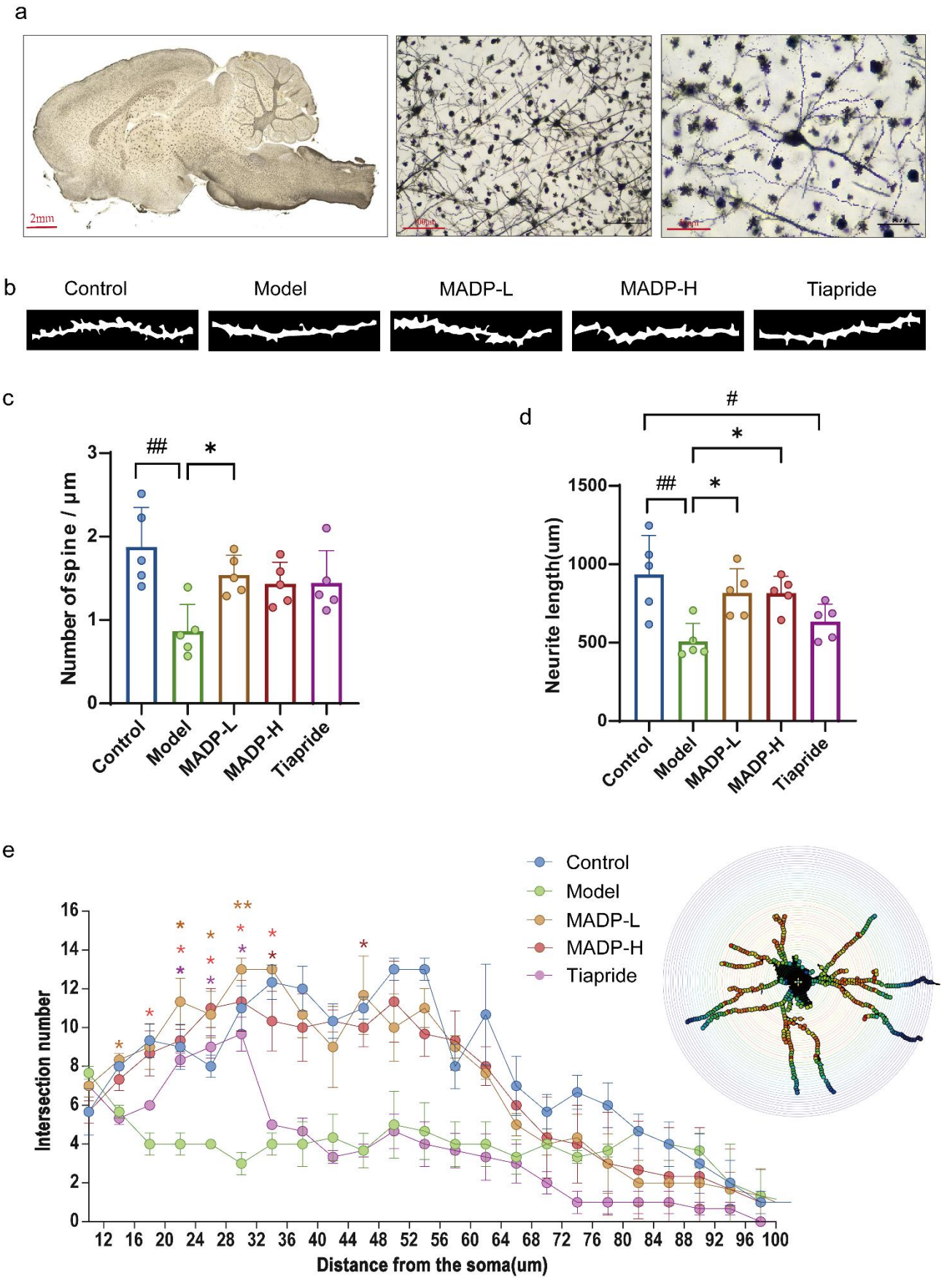


Fig. 5 Representative images of Nissl staining in coronal sections of the PFC across experimental groups

(a) In the Control group, the cortex exhibited an intact tissue structure with clear stratification. Pyramidal neurons showed a regular morphology and plump cell bodies, with deep-blue stained Nissl bodies. (b) In the Model group, neurons displayed disorganized alignment, pale cytoplasmic staining, and cellular swelling or pyknosis. (c) MADP-L attenuated brain tissue injury, characterized by distinct neuronal layers, intact pyramidal cell morphology, and deepened Nissl body staining. (d) In the MADP-H group, neurons restored arrangement, Nissl bodies re-aggregated, and tissue edema was reduced. (e) The Tiapride group also demonstrated neuroprotective effects, with improved neuronal alignment and deepened Nissl body staining, although some neurons still exhibited blurred outlines. Scale bar = 200 μm. Data are presented as means ± SEM. The notation ns signifies no significant difference. Statistical analysis for Section F was performed using one-way ANOVA followed by Tukey's multiple-comparisons test.

3.4. Golgi staining

The results showed that dendritic spine density in the PFC of the model group was significantly reduced ($P<0.05$; Fig. 6c). IDPN combined with CRS induced significant alterations in the dendritic morphology of PFC neurons, with a notable reduction in the total number of intersections and total neurite length ($P<0.05$; Fig. 6d–e). Notably, treatment with MADP restored the impaired dendritic spine density and dendritic morphology ($P<0.05$).


a
2mm
b
Control
Model
MADP-L
MADP-H
Tiapride
c
Number of spine / μm
##
*
Control
Model
MADP-L
MADP-H
Tiapride
d
Neurite length(um)
#
*
##
*
e
Control
Model
MADP-L
MADP-H
Tiapride
Intersection number
Distance from the soma(um)

310

Fig. 6 Representative images of Golgi staining in the PFC across experimental groups
(a) Sagittal section of the brain and profile image of Golgi staining in the PFC, demonstrating the impregnation of neurons. (b) Representative images of dendritic segments from the PFC. Scale bar = 20 μm. (c) Dendritic spine density of neurons in each group. (d) Total neurite length of neurons in each group. (e) Sholl plot illustrating the complexity of dendritic arbor branching. The x-axis represents the distance from the soma, while the y-axis represents the number of intersections between the tracing and Sholl shells. Data are presented as means ± SEM (n = 5 per group, with 10 neurons analyzed per animal). The notation #$p < 0.05$ and ##$p < 0.01$ indicate a comparison with the Control group. Conversely, *$p < 0.05$ and **$p < 0.01$ refer to comparisons with the Model group. Sections c–d were assessed using one-way ANOVA followed by Tukey's multiple-comparisons test, while section E was evaluated through two-way ANOVA alongside Tukey's multiple-comparisons test.

3.5. Network pharmacology

To further investigate the multi-component and multi-target network of the formula, network pharmacology was employed to predict the potential targets of MADP. Based on the 135 constituents identified via UPLC-MS/MS, a total of 853 potential biological targets were predicted using the SwissTargetPrediction database (Supplementary Table S2). Concurrently, 1,909 genes associated with TS and anxiety were retrieved from five public databases. Intersection analysis between MADP targets and disease-related genes yielded 303 common targets (Fig. 7a). The compound-disease target network comprised 436 nodes and 2,376 edges, intuitively illustrating the multi-component and multi-target therapeutic profile of MADP (Fig. 7b).
The 303 intersecting targets were imported into the STRING database to construct a PPI network. Utilizing the CytoNCA plugin in Cytoscape, 74 hub targets were identified through topological screening, including PRKACA, TP53, and PIK3CA (Fig. 7c and Supplementary Table S3). Functional enrichment analysis was performed on these 74 hub targets. GO enrichment involved 2,723 biological processes (BP; e.g., regulation of membrane potential), 173 cellular components (CC; e.g., synaptic membrane), and 395 molecular functions (MF; e.g., neuroactive ligand-receptor interaction) (Fig. 7e). Furthermore, KEGG pathway enrichment identified 181 pathways, indicating that the cAMP signaling pathway is a critical pathway for MADP in the treatment of TD (Fig. 7d).

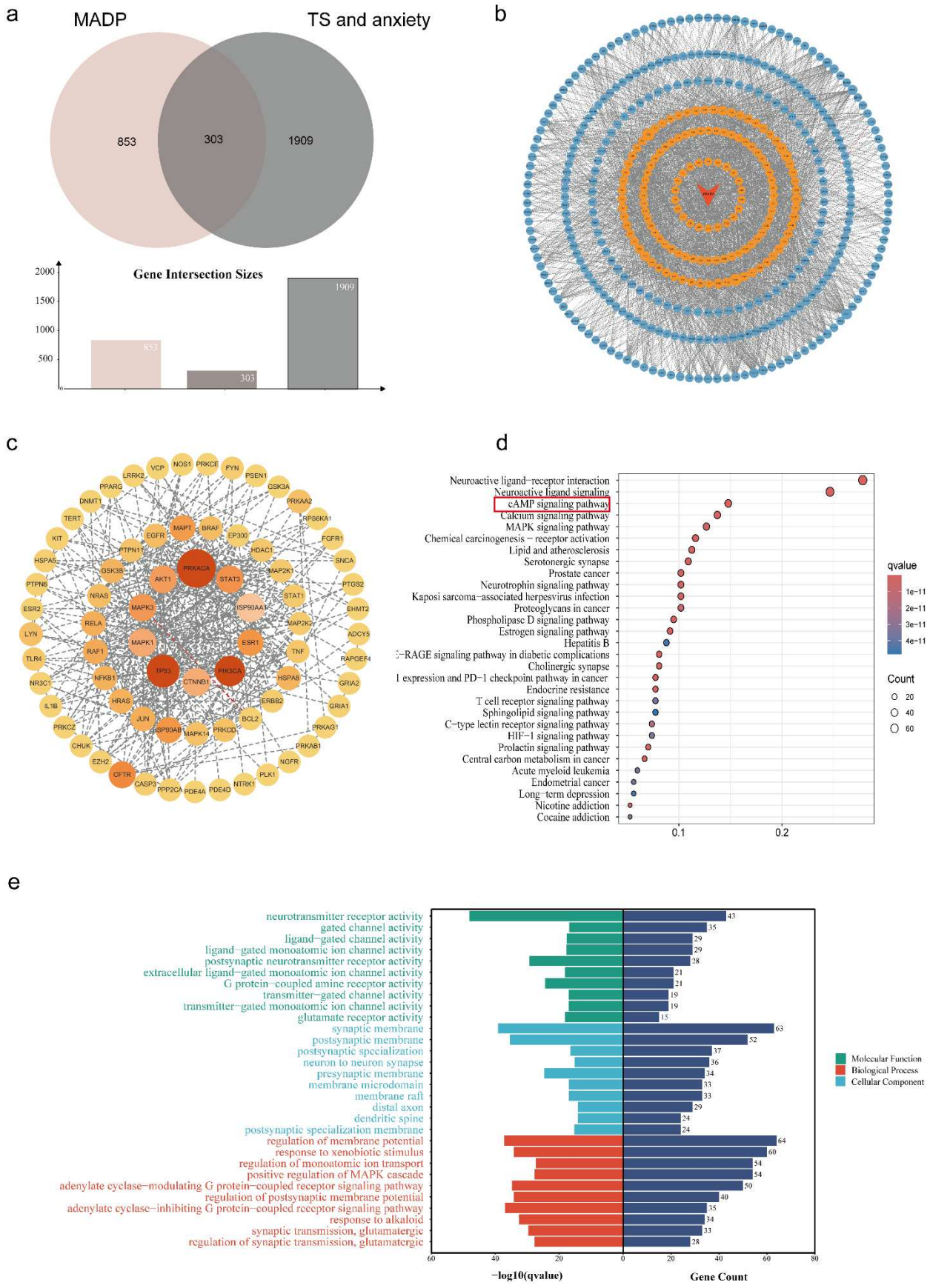


Fig. 7 Network pharmacology analysis of MADP for treating TS comorbid with anxiety

(a) Venn diagram of 303 intersecting genes between MADP-related targets and targets associated with TS and anxiety. (b) Composite target network of potential therapeutic targets for MADP. The yellow rhombus node indicates MADP; orange circle nodes represent the active ingredients in MADP; and blue circle nodes represent the potential action targets. (c) PPI network of the intersecting genes. Hub targets were screened based on nodes with parameters exceeding the median values of BC, CC, DC, EC, LAC, and NC. A larger degree value is indicated by a darker color and a larger node size. (d) Bubble chart of KEGG pathway enrichment analysis for the potential therapeutic targets. (e) Bar chart of GO enrichment analysis for potential therapeutic targets, covering BP, CC, and MF.

3.6. Transcriptomic analysis

To validate the potential therapeutic targets of MADP, mRNA sequencing was performed on PFC tissues from the control, model, and MADP-L groups. Results revealed 170 differentially expressed (DE) mRNAs in the model group compared with the control group (84 downregulated and 86 upregulated). Meanwhile, 251 DE mRNAs (166 downregulated and 85 upregulated) were identified in the MADP group compared to the model group.

Functional enrichment analysis was conducted on these DE mRNAs. GO enrichment showed that the DEGs were significantly associated with neuronal excitability and endocrine homeostasis, including terms such as G-protein-coupled receptor activity, ion-gated channel activity, and regulation of hormone secretion. Furthermore, KEGG pathway analysis indicated that these genes were primarily enriched in the calcium signaling pathway, neuroactive ligand-receptor interaction, and cAMP signaling pathway. Detailed results are presented in Figure 8.

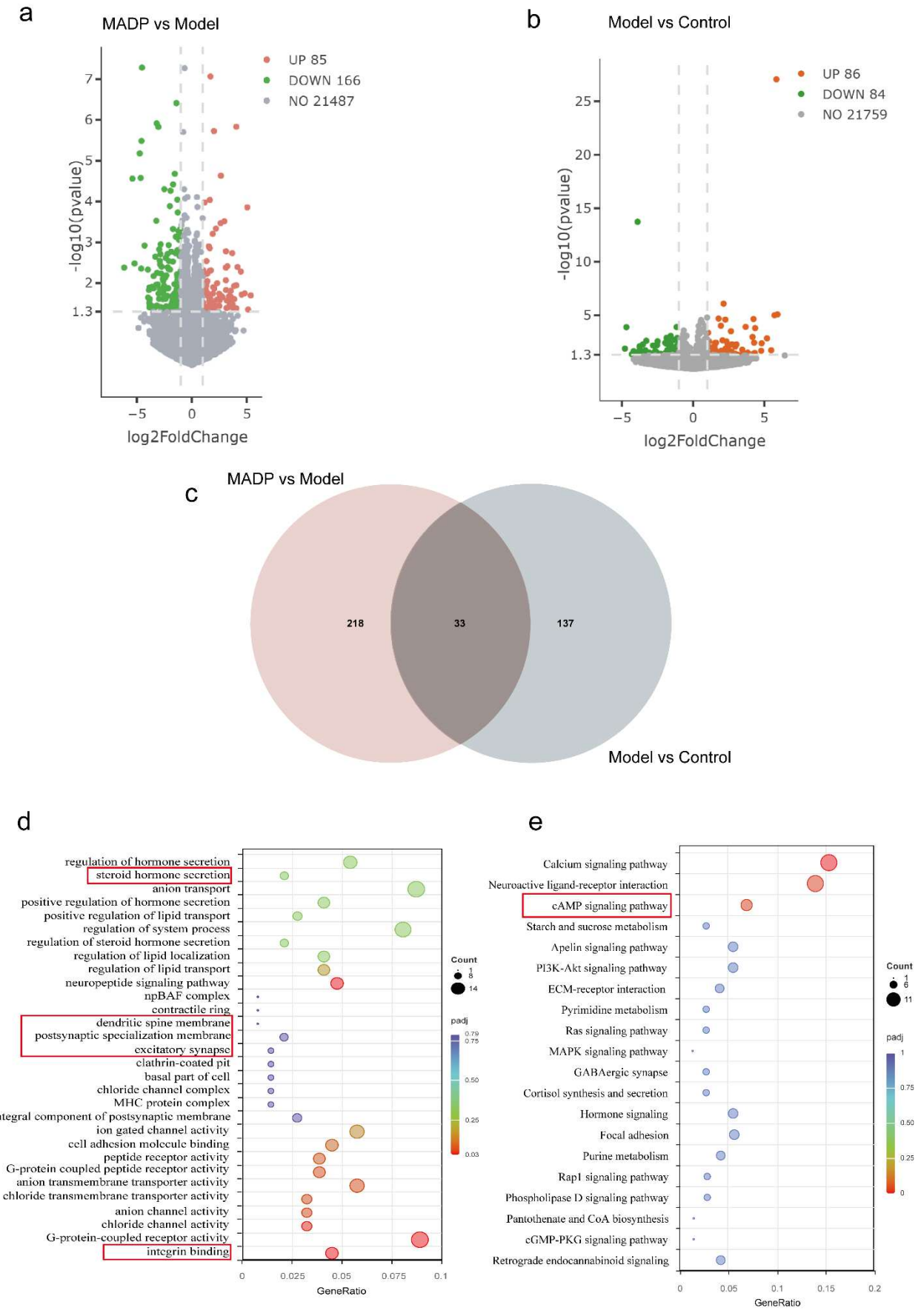

a
MADP vs Model
UP 85
DOWN 166
NO 21487
-log10(pvalue)
log2FoldChange
b
Model vs Control
UP 86
DOWN 84
NO 21759
-log10(pvalue)
log2FoldChange
c
MADP vs Model
218
33
137
Model vs Control
d
regulation of hormone secretion
steroid hormone secretion
anion transport
positive regulation of hormone secretion
positive regulation of lipid transport
regulation of system process
regulation of steroid hormone secretion
regulation of lipid localization
regulation of lipid transport
neuropeptide signaling pathway
npBAF complex
contractile ring
dendritic spine membrane
postsynaptic specialization membrane
excitatory synapse
clathrin-coated pit
basal part of cell
chloride channel complex
MHC protein complex
integral component of postsynaptic membrane
ion gated channel activity
cell adhesion molecule binding
peptide receptor activity
G-protein coupled peptide receptor activity
anion transmembrane transporter activity
chloride transmembrane transporter activity
anion channel activity
chloride channel activity
G-protein-coupled receptor activity
integrin binding
GeneRatio
Count
padj
e
Calcium signaling pathway
Neuroactive ligand-receptor interaction
cAMP signaling pathway
Starch and sucrose metabolism
Apelin signaling pathway
PI3K-Akt signaling pathway
ECM-receptor interaction
Pyrimidine metabolism
Ras signaling pathway
MAPK signaling pathway
GABAergic synapse
Cortisol synthesis and secretion
Hormone signaling
Focal adhesion
Purine metabolism
Rap1 signaling pathway
Phospholipase D signaling pathway
Pantothenate and CoA biosynthesis
cGMP-PKG signaling pathway
Retrograde endocannabinoid signaling
GeneRatio
Count
padj

Fig. 8 mRNA sequencing results of PFC tissues across Control, Model, and MADP-L groups (n = 4) (a) Volcano plot of DE mRNAs in the MADP vs. Model group. (b) Volcano plot of DE mRNAs in the Model vs. Control group. (c) Venn diagram of DE mRNAs among the three groups. (d) GO functional enrichment analysis of the differentially expressed genes. (e) KEGG pathway enrichment analysis of the differentially expressed genes.

3.7. Western blot validation of the cAMP/PKA/CREB signaling pathway

To further validate the potential mechanisms identified through transcriptomic analysis, the effects of MADP on the total and phosphorylated protein levels of PKA and CREB in the PFC were evaluated (Fig. 9). MADP treatment significantly increased the total protein levels of PKA and CREB, as well as the phosphorylation of CREB ($P<0.05$); however, no significant alterations were observed in the expression of p-PKA ($P>0.05$). The therapeutic effects of the low- and high-dose MADP groups were consistent and did not exhibit a dose-dependent manner.

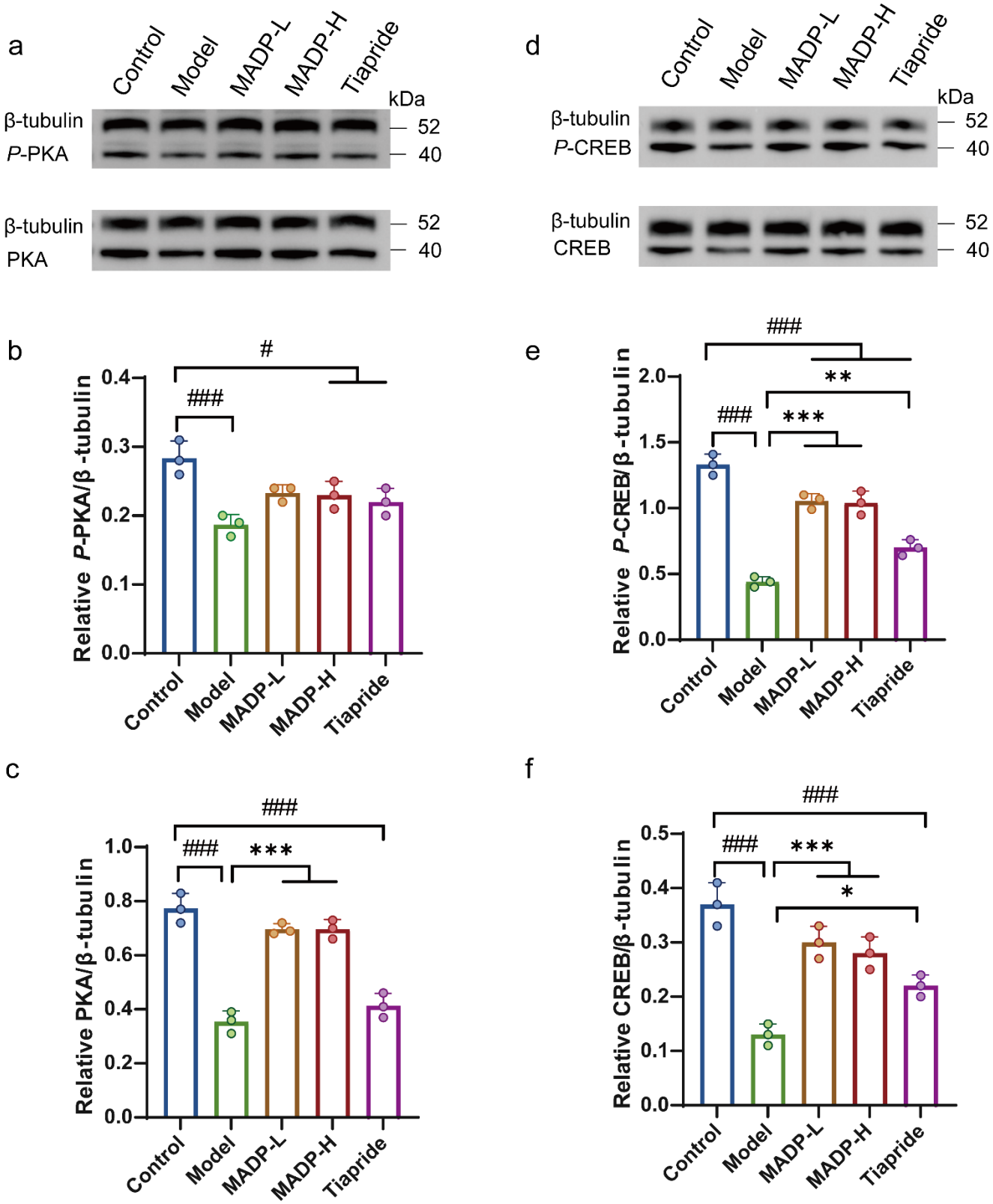


Fig. 9 Impact of MADP on the PKA/CREB pathway in the PFC

(a–c) Western blot analysis of PKA and p-PKA protein levels in rat PFC tissues. PKA and p-PKA levels were normalized to β-tubulin as the internal control (n = 3). (d–f) Western blot analysis of CREB and p-CREB protein levels in rat PFC tissues. CREB and p-CREB levels were normalized to β-tubulin (n = 3). The notation #$p < 0.05$ and ###$p < 0.001$ indicate a comparison with the Control group.

Conversely, *$p < 0.05$, **$p < 0.01$ and ***$p < 0.001$ refer to comparisons with the Model group. All data were assessed using one-way ANOVA followed by Tukey's multiple-comparisons test.

3.8. Immunofluorescence analysis of synaptic markers

To evaluate synaptic transmission efficacy, we examined the expression of synaptic markers in the PFC. The results demonstrated that IDPN combined with chronic stress induced a significant reduction in the fluorescence intensity of the presynaptic marker Synapsin I+II and the postsynaptic marker PSD95 ($P < 0.05$). Notably, MADP treatment significantly elevated the expression levels of both PSD95 and Synapsin I+II within these PFC regions ($P < 0.05$; Fig. 10).

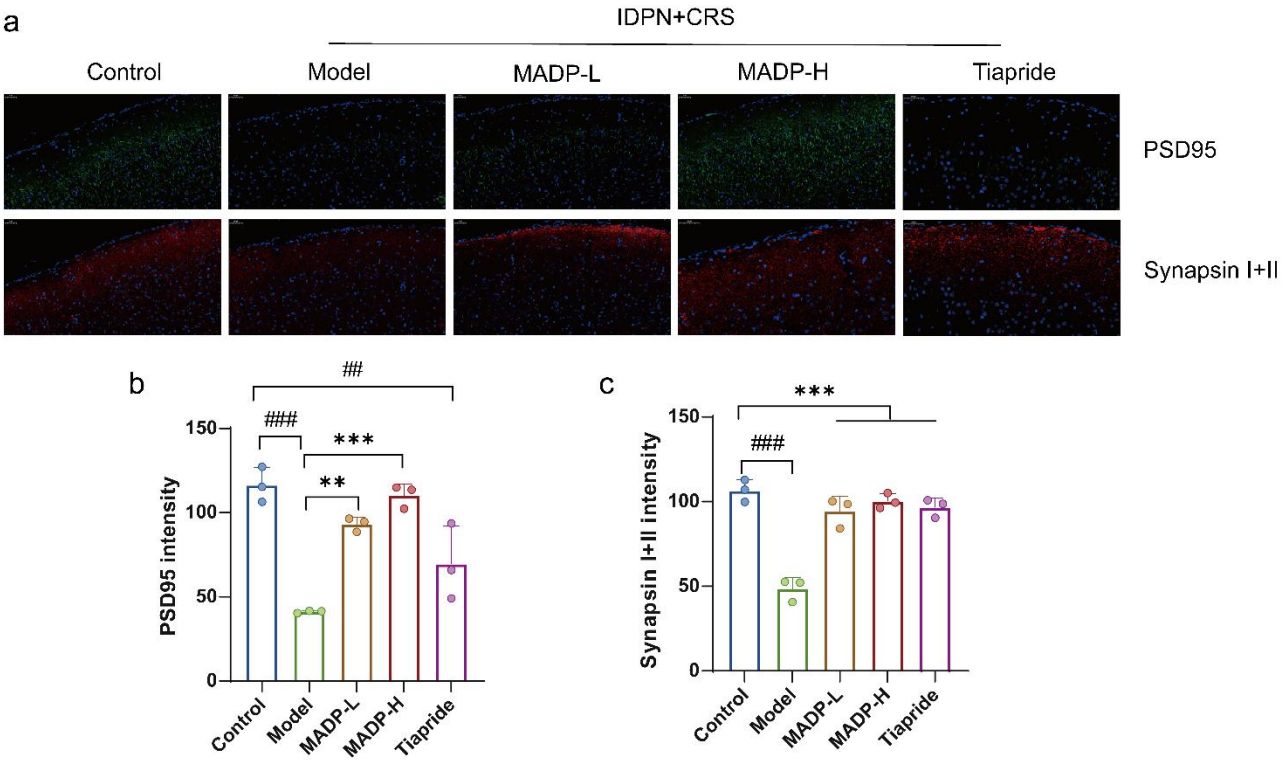


Fig. 10 Impact of MADP on synaptic marker proteins in the PFC
(a) Representative immunofluorescence images illustrating the effects on PSD95 (green) and Synapsin I+II (red) across experimental groups. Scale bar = 50 μm. (b–c) Statistical quantification of PSD95 and Synapsin I+II expression density. The notation ##$p < 0.01$ and ###$p < 0.001$ indicate a comparison with the Control group. Conversely, **$p < 0.01$ and ***$p < 0.001$ refer to comparisons with the Model group. All data were assessed using one-way ANOVA followed by Tukey's multiple-comparisons test.

4. Discussion

This study successfully established an IDPN- and CRS-induced rat model of TS comorbid with anxiety. We demonstrated that MADP effectively alleviated stereotypic behaviors and restored synaptic plasticity within PFC neurons. By integrating UPLC-MS, network pharmacology, and transcriptomics, we identified the cAMP/PKA/CREB signaling pathway as a key mediator of MADP's therapeutic effects (Fig. 11). Crucially, Western blot and immunofluorescence validations corroborate these findings, establishing a clear mechanistic basis for utilizing MADP to treat TS.

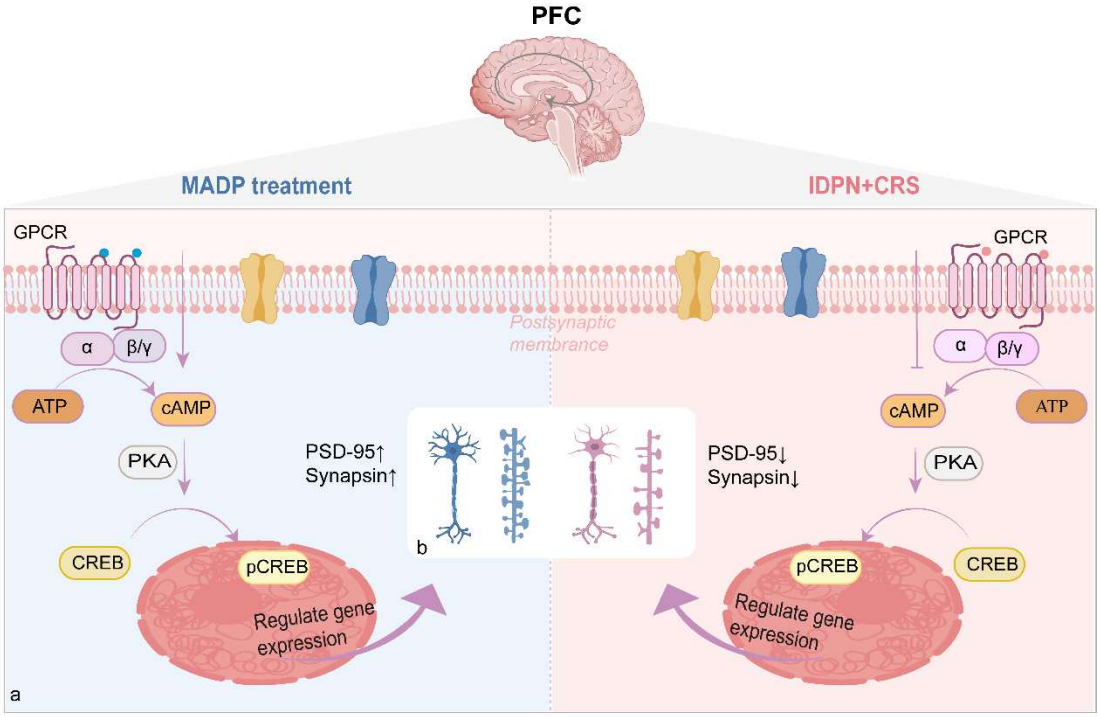


Fig. 11 Schematic diagram of the mechanism by which MADP regulates the cAMP/PKA/CREB signaling pathway and synaptic plasticity

(a) cAMP/PKA/CREB signaling cascade. (b) Alterations in synaptic plasticity.

Clinically, chronic stress (e.g., prolonged pressure and tension) is not only a primary inducer of anxiety but also a critical factor triggering and exacerbating TS symptoms.[21,22] While acute, moderate stress represents an adaptive mechanism to environmental changes that can enhance synaptic transmission, chronic or unpredictable excessive stress impairs synaptic plasticity, leading to the development of neuropsychiatric conditions. Within the central nervous system, the PFC is exceptionally sensitive to stress; CRS has been pathologically shown to cause the shrinkage of mature dendritic spines in PFC, thereby diminishing their conductive properties.[23] Consistently, our study demonstrated that IDPN combined with CRS induced significant alterations in dendritic spine density, total neurite length, and dendritic arbor complexity in PFC neurons. Therapeutically, activation of the PFC attenuates anxiety- and depressive-like behaviors, providing further evidence for its critical involvement in emotional regulation.[24]

As a "top-down" regulatory hub, the PFC modulates behavioral motivation and motor execution through glutamatergic projections to the striatum, suggesting that PFC dysfunction is intimately associated with the hyperkinesia observed in TS.[25] Moreover, in chronic stress models, the connection between the PFC and inhibitory parvalbumin interneurons is weakened, while signaling in the striatal direct pathway is enhanced, triggering motor hyperactivity.[26] Clinical evidence further supports these findings. MRI studies have revealed cortical thinning and volume reduction in the PFC of children

with TS,[27,28] and activation of the PFC has been shown to modulate the inhibitory control of obsessive-compulsive symptoms.[29] Collectively, these findings suggest that stress-induced PFC dysfunction may constitute a common pathological bridge between tics and anxiety.

In TCM, tics are viewed as manifestations of internal liver wind agitation, while disturbance of *Shen* (spirit) serves as the common pathological foundation for both TS and anxiety. TS and anxiety interact reciprocally, establishing a vicious cycle of emotional stimuli, tics, psychological distress, and clinical exacerbation. Within the MADP formula, *Scutellaria baicalensis*, *Paeonia lactiflora*, and *Cassia obtusifolia* are utilized to soothe, soften, and clear the liver, while *Curcuma wenyujin*, *Acorus tatarinowii*, and *Polygala tenuifolia* serve to alleviate depression, open the orifices, and tranquilize the *Shen*. This dual-therapeutic approach aims to regulate the patient's emotional state while mitigating tics, thereby disrupting the bidirectional deleterious cycle. Consistently, our study demonstrated that MADP effectively attenuated stereotypic behaviors and restored synaptic plasticity impairment in PFC neurons under stress. Integrated network pharmacology and multi-omics analysis further revealed that these neuroprotective effects are potentially mediated via the cAMP/PKA/CREB signaling pathway.

Within neurons, the cAMP/PKA/CREB pathway serves as a canonical molecular foundation for regulating dendritic spine morphology, neurotransmitter receptor function, and downstream gene expression.[30] Chronic stress triggers neurotransmitter dysregulation in the PFC, leading to the under-activation of G-protein-coupled receptors and the cAMP/PKA cascade, which subsequently impairs CREB-mediated protein synthesis. This transcriptional block reduces the synthesis of proteins essential for maintaining synaptic structure and function (such as PSD-95, Synapsin, and GluA1) resulting in PFC neuroplasticity dysregulation.[24,31] Previous research indicated that volatile oil from *Acorus tatarinowii* enhances synaptic plasticity and improves tics in TS rats via activation of the CaMKII/CREB pathway.[32] Consistently, *Acorus tatarinowii* essential oils modulate the cAMP/PKA/CREB pathway to ameliorate depressive-like behaviors.[33] *Scutellaria baicalensis* can reverse stress-induced declines in CaMKII and CREB levels while downregulating the aberrant elevation of Cav1.2 (L-type calcium channels) to restore neuroplasticity.[34] Furthermore, *Scutellariae Radix* repairs prenatal stress-induced neurodevelopmental disorders by improving hippocampal neurogenesis and regulating neurobiochemical factors.[35] As these medicinal herbs and monomeric constituents are core ingredients of MADP, these findings underscore the formula's regulatory influence on the cAMP/PKA/CREB signaling pathway and synaptic plasticity.

Given the inherent complexity of TCM preparations, our research primarily focused on the holistic effects of MADP, yet the therapeutic mechanisms remain to be fully elucidated at the monomer or specific component level. Future investigations should prioritize the detection of blood-entering and brain-penetrating components to clarify the precise pharmacological material basis of the formula. Additionally, while network pharmacology provides valuable predictions, subsequent studies should incorporate molecular docking to verify the direct binding affinity between core active ingredients and hub targets. Although the animal model successfully simulated core symptoms, it may not fully capture the inter-individual heterogeneity observed in clinical patients. Notably, the excessive stereotypic behaviors in the IDPN+CRS model potentially interfered with anxiety assessments in the OFT, suggesting that TS-comorbid anxiety may differ phenotypically from isolated anxiety. Therefore, more diverse behavioral paradigms, such as the elevated plus-maze, tail suspension test and forced swim test, should be employed for a more comprehensive evaluation. Finally, the underlying mechanisms of MADP warrant further validation through in vitro assays and the use of specific pathway inhibitors or activators to rigorously confirm its regulatory effects.

5. Conclusion

In summary, the study reveals that MADP effectively restores PFC synaptic impairment induced by IDPN combined with CRS. This therapeutic mechanism is intimately associated with the activation of the cAMP/PKA/CREB signaling pathway and the subsequent regulation of synapse-related proteins. These findings provide novel theoretical support and a scientific basis for the clinical application of MADP in the treatment of TS comorbid with anxiety.

References

1. Leibu E, First MB. DSM-5. Mount Sinai Expert Guides2016. p. 1-8.
2. Hirschtritt ME, Lee PC, Pauls DL, Dion Y, Grados MA, Illmann C, et al. Lifetime prevalence, age of risk, and genetic relationships of comorbid psychiatric disorders in Tourette syndrome. JAMA Psychiatry. 2015;72(4):325-33. doi: 10.1001/jamapsychiatry.2014.2650. PubMed PMID: 25671412; PubMed Central PMCID: PMCQ1.
3. Yang Z, Wu H, Lee PH, Tsetsos F, Davis LK, Yu D, et al. Investigating Shared Genetic Basis Across Tourette Syndrome and Comorbid Neurodevelopmental Disorders Along the Impulsivity-Compulsivity Spectrum. Biological Psychiatry. 2021;90(5):317-27. doi: 10.1016/j.biopsych.2020.12.028. PubMed PMID: 33714545; PubMed Central PMCID: PMCQ1.
4. Bernard BA, Stebbins GT, Siegel S, Schultz TM, Hays C, Morrissey MJ, et al. Determinants of quality of life in children with Gilles de la Tourette syndrome. Movement Disorders : Official Journal of the Movement Disorder Society. 2009;24(7):1070-3. doi: 10.1002/mds.22487. PubMed PMID: 19306279; PubMed Central PMCID: PMCQ1.
5. Zhang S, Han F, Chen J, Shen X, Li Y. Clinical Features, Mechanisms, and Management of Anxiety in Youth with Tic Disorders: A Narrative Review. Neuropsychiatr Dis Treat. 2026;22:582875. Epub 20260303. doi: 10.2147/ndt.S582875. PubMed PMID: 41798289; PubMed Central PMCID: PMCPMC12967050.
6. Robertson MM. Mood disorders and Gilles de la Tourette's syndrome: An update on prevalence, etiology, comorbidity, clinical associations, and implications. J Psychosom Res. 2006;61(3):349-58. PubMed PMID: 16938513; PubMed Central PMCID: PMCQ2.
7. Fernández de la Cruz L, Rydell M, Runeson B, Brander G, Rück C, D'Onofrio BM, et al. Suicide in Tourette's and Chronic Tic Disorders. Biological Psychiatry. 2017;82(2):111-8. doi: 10.1016/j.biopsych.2016.08.023. PubMed PMID: 27773353; PubMed Central PMCID: PMCQ1.
8. Berzosa-Gonzalez I, Martinez-Horta S, Pérez-Pérez J, Kulisevsky J, Pagonabarraga J. Therapeutic Approach to Primary Tic Disorders and Associated Psychiatric Comorbidities. Brain Sciences. 2024;14(12). doi: 10.3390/brainsci14121231. PubMed PMID: 39766430; PubMed Central PMCID: PMCQ3.
9. Li Y, Pan C, Han X M. Clinical observation on 32 cases of Tourette's syndrome in children treated by acupuncture combined with medicine. Hunan J Tradit Chin Med. 2021; 37(5): 97-98, 111. doi:10.16808/j.cnki.issn1003-7705.2021.05.033
10. Li Y, Liu D, Pan C. Observation of the efficacy of Anshen Dingzhi formula combined with vitamin D3 drops in the treatment of children with tic disorder. Shenzhen J Integr Tradit Chin West Med. 2025; 35(3): 1-4. doi:10.16458/j.cnki.1007-0893.2025.03.001
11. Tian X, Ou G, Hu S, Wang C, Han F, Gao L. Integrated network pharmacology and experimental verification to explore the molecular mechanism of Jingxin Zhidong formula for treating Tic disorder.

Journal of Ethnopharmacology. 2023;305:116114. doi: 10.1016/j.jep.2022.116114. PubMed PMID: 36587455; PubMed Central PMCID: PMCQ1.
12. Hu J, Li H, Wang X, Cheng H, Zhu G, Yang S. Novel mechanisms of Anshen Dingzhi prescription against PTSD: Inhibiting DCC to modulate synaptic function and inflammatory responses. Journal of Ethnopharmacology. 2024;333:118425. doi: 10.1016/j.jep.2024.118425. PubMed PMID: 38848974; PubMed Central PMCID: PMCQ1.
13. Yang S, Qu Y, Wang J, Gao F, Ji M, Xie P, et al. Anshen Dingzhi prescription in the treatment of PTSD in mice: Investigation of the underlying mechanism from the perspective of hippocampal synaptic function. Phytomedicine : International Journal of Phytotherapy and Phytopharmacology. 2022;101:154139. doi: 10.1016/j.phymed.2022.154139. PubMed PMID: 35523115; PubMed Central PMCID: PMCQ1.
14. Lin J, Zhang Y, Sun Q, Zhang F, Song R, Wang X, et al. Acori Tatarinowii Rhizoma-Curcumae Radix Herbal pair ameliorates depression by regulating microglia M1/M2 polarization via TLR4/MyD88/NF-κB pathway. Journal of Ethnopharmacology. 2025;356:120825. doi: 10.1016/j.jep.2025.120825. PubMed PMID: 41173083; PubMed Central PMCID: PMCQ1.
15. Wang C, Xu X, Zhu H, Wu D, Liang J, Wang X, et al. Acori tatarinowii Rhizoma-Curcumae Radix herbal pair ameliorates cognitive impairment and suppresses neuro-inflammation via Ca2+/CaMKKβ/AMPK/mTOR pathway in Alzheimer's disease. Journal of Ethnopharmacology. 2026;365:121606. doi: 10.1016/j.jep.2026.121606. PubMed PMID: 41916153; PubMed Central PMCID: PMCQ1.
16. Zhu L, Ma S, Li K, Xiong P, Qin S, Cai W. Systematic Screening of Chemical Constituents in the Traditional Chinese Medicine Arnebiae Radix by UHPLC-Q-Exactive Orbitrap Mass Spectrometry. Molecules. 2022;27(9). doi: 10.3390/molecules27092631. PubMed PMID: 35565981; PubMed Central PMCID: PMCQ2.
17. Knott PJ, Hutson PH. Stress-induced stereotypy in the rat: neuropharmacological similarities to Tourette syndrome. Adv Neurol. 1982;35:233-8. PubMed PMID: 6983245.
18. Zhang W, Yu W, Liu X, Wang Q, Bai X, Cui X, et al. Effect of Jian-Pi-Zhi-Dong Decoction on the Amino Acid Neurotransmitters in a Rat Model of Tourette Syndrome and Comorbid Anxiety Disorder. Frontiers In Psychiatry. 2020;11:515. doi: 10.3389/fpsyt.2020.00515. PubMed PMID: 32581885; PubMed Central PMCID: PMCQ2.
19. Zhang N, Zhang H, Guo J, Ma Y, Bai X, Ma N, et al. Exploring the Therapeutic Mechanism of Jianpi Zhidong Decoction on Tourette Syndrome Based on Proteomics and Network Pharmacology. Drug Des Devel Ther. 2025;19:3139-58. doi: 10.2147/DDDT.S505173. PubMed PMID: 40291161; PubMed Central PMCID: PMCQ1.
20. Fan F, Zhang S, Wu H, Zhang M, Han F. Modulatory Effects of Jujuboside A on Amino Acid Neurotransmitter Profiles in Tic Disorder. Brain and Behavior. 2025;15(11):e71041. doi: 10.1002/brb3.71041. PubMed PMID: 41220182; PubMed Central PMCID: PMCQ2.
21. Barber KE, Ding Q, Espil FM, Woods DW, Specht MW, Bennett SM, et al. Contextual Triggers and Tic Severity Across Life Periods: A Retrospective Analysis in Adults with Tic Disorders. Child Psychiatry Hum Dev. 2024. doi: 10.1007/s10578-024-01733-y. PubMed PMID: 38976153; PubMed Central PMCID: PMCQ2.
22. Godar SC, Bortolato M. What makes you tic? Translational approaches to study the role of stress and contextual triggers in Tourette syndrome. Neuroscience and Biobehavioral Reviews. 2016;76(Pt

A):123-33. doi: 10.1016/j.neubiorev.2016.10.003. PubMed PMID: 27939782; PubMed Central PMCID: PMCQ1.
23. Mayanagi T, Sobue K. Social Stress-Induced Postsynaptic Hyporesponsiveness in Glutamatergic Synapses Is Mediated by PSD-Zip70-Rap2 Pathway and Relates to Anxiety-Like Behaviors. Front Cell Neurosci. 2020;13:564. doi: 10.3389/fncel.2019.00564. PubMed PMID: 31969804; PubMed Central PMCID: PMCQ2.
24. Page CE, Coutellier L. Prefrontal excitatory/inhibitory balance in stress and emotional disorders: Evidence for over-inhibition. Neuroscience and Biobehavioral Reviews. 2019;105:39-51. doi: 10.1016/j.neubiorev.2019.07.024. PubMed PMID: 31377218; PubMed Central PMCID: PMCQ1.
25. Lin K, Coutellier L. Evidence for the involvement of a fronto-striatal pathway in the processing of social reward. Prog Neurobiol. 2025;254:102834. doi: 10.1016/j.pneurobio.2025.102834. PubMed PMID: 41072650; PubMed Central PMCID: PMCQ1.
26. Rodrigues D, Monteiro P. Chronic stress promotes basal ganglia disinhibition by increasing the excitatory drive of direct-pathway neurons. Neurobiol Stress. 2023;27:100571. doi: 10.1016/j.ynstr.2023.100571. PubMed PMID: 37781564; PubMed Central PMCID: PMCQ2.
27. Greene DJ, Williams Iii AC, Koller JM, Schlaggar BL, Black KJ. Brain structure in pediatric Tourette syndrome. Molecular Psychiatry. 2016;22(7):972-80. doi: 10.1038/mp.2016.194. PubMed PMID: 27777415; PubMed Central PMCID: PMCQ1.
28. Liu Y, Miao W, Wang J, Gao P, Yin G, Zhang L, et al. Structural abnormalities in early Tourette syndrome children: a combined voxel-based morphometry and tract-based spatial statistics study. PloS One. 2013;8(9):e76105. doi: 10.1371/journal.pone.0076105. PubMed PMID: 24098769; PubMed Central PMCID: PMCQ2.
29. Lopez-Sosa F, Reneses B, Sanmartino F, Galarza-Vallejo A, Garcia-Albea J, Cruz-Gomez AJ, et al. Nucleus Accumbens Stimulation Modulates Inhibitory Control by Right Prefrontal Cortex Activation in Obsessive-Compulsive Disorder. Cerebral Cortex (New York, NY : 1991). 2021;31(5):2742-58. doi: 10.1093/cercor/bhaa397. PubMed PMID: 33406245; PubMed Central PMCID: PMCQ2.
30. Bhattacharya A, Turkalj L, Manzini MC. The promise of cyclic AMP modulation to restore cognitive function in neurodevelopmental disorders. Curr Opin Neurobiol. 2024;90:102966. doi: 10.1016/j.conb.2024.102966. PubMed PMID: 39740265; PubMed Central PMCID: PMCQ1.
31. Ren B, Yuan Q, Cha S, Liu S, Zhang J, Guo G. Maladaptive Neuroplasticity Under Stress: Insights into Neuronal and Synaptic Changes in the Prefrontal Cortex. Mol Neurobiol. 2025;62(11):15227-49. doi: 10.1007/s12035-025-05152-5. PubMed PMID: 40545507; PubMed Central PMCID: PMCQ1.
32. Feng P, Chen Y, Sun K, Wei X, Ding Y, Shang J, et al. Volatile oil from Acori graminei Rhizoma affected the synaptic plasticity of rats with tic disorders by modulating dopaminergic and glutamatergic systems. Journal of Ethnopharmacology. 2024;335:118676. doi: 10.1016/j.jep.2024.118676. PubMed PMID: 39147000; PubMed Central PMCID: PMCQ1.
33. Zhang S, Hu Y, Zhao Y, Feng Y, Wang X, Miao M, et al. Molecular mechanism of Chang Shen Hua volatile oil modulating brain cAMP-PKA-CREB pathway to improve depression-like behavior in rats. Phytomedicine : International Journal of Phytotherapy and Phytopharmacology. 2024;130:155729. doi: 10.1016/j.phymed.2024.155729. PubMed PMID: 38772184; PubMed Central PMCID: PMCQ1.
34. Lv B, Cao K, Chen Z, Zhong J, Wang K, Zhang R, et al. Jieyu I formula and its primary component quercetin alleviate anxiety by modulating neuroregeneration and inflammation via the calcium

signaling pathway. Journal of Ethnopharmacology. 2025;356:120820. doi: 10.1016/j.jep.2025.120820. PubMed PMID: 41173084; PubMed Central PMCID: PMCQ1.
35. Li L, Zhang W, Sun C, Chai Z, Wang K, Zhou Q, et al. <italic>Scutellariae radix</italic> Ameliorates Prenatal Stress-Induced Anxiety-Like and Depression-Like Behavior in the Offspring via Reversing HPA Axis Hyperfunction and Ameliorating Neurodevelopmental Dysfunction. Dev Neurosci. 2024;47(6):421-39. doi: 10.1159/000543152. PubMed PMID: 39701046; PubMed Central PMCID: PMCQ3.

Statements and Declarations

Funding
This work was supported by the Natural Science Foundation of Nanjing University of Chinese Medicine (No. XZR2024264) and the "Science and Education for Health" Project of Suzhou Municipal Health Commission (No. QNXM2025047).

Competing Interests
The authors declare no competing financial or non-financial interests.

Ethics Approval
All animal experimental protocols were reviewed and approved by the Experimental Animal Ethics Committee of Nanjing University of Chinese Medicine.

Author Contributions
All authors contributed to the study conception and design. Material preparation, data collection and analysis were performed by Si Zhang, Lixiang Zhang, Yan Li, Mei Li, Jie Chen, Liang Li, Fei Fan, Xiaohua Shen, and Guoqiang Liang. The first draft of the manuscript was written by Si Zhang. Lingling Yang and Guoqiang Liang supervised the study and critically revised the manuscript. All authors commented on previous versions of the manuscript. All authors read and approved the final manuscript.

Data Availability
The raw RNA-sequencing data and the processed expression matrix generated during the current study have been deposited in the NCBI Gene Expression Omnibus (GEO) database and are publicly accessible under the accession number GSE335737 (https://www.ncbi.nlm.nih.gov/geo/query/acc.cgi?acc=GSE335737).

Acknowledgments
The authors gratefully acknowledge the Children's Hospital of Soochow University for providing the experimental platform.

Supplementary Files

This is a list of supplementary files associated with this preprint. Click to download.

- SupplementaryTableS1.xlsx
- SupplementaryTableS2.xlsx
- SupplementaryTableS3.xlsx